2009 American Control Conference
Hyatt Regency Riverfront, St. Louis, MO, USA
June 10-12, 2009

Melt Pool Temperature Modeling and Control for Laser Metal Deposition Processes

Lie Tang and Robert G. Landers
Department of Mechanical and Aerospace Engineering
Missouri University of Science and Technology
400 West 13th Street, Rolla, Missouri 65409–0050
{ltx8d,landersr}@mst.edu

***Abstract*—Melt pool temperature is of great importance to deposition quality in Laser Metal Deposition processes. To control the melt pool temperature, an empirical process model describing the relation between the temperature and laser power, powder flow rate, and traverse speed is established and verified experimentally. A general tracking controller using the Internal Model Principle is then designed. To examine the controller performance, two experiments tracking a constant temperature reference and a time varying reference are conducted. The results are compared to open–loop experiments where the laser power profile is derived directly from the model. The results show the melt pool temperature controller performs well in tracking both constant and time varying references and that the closed-loop control system greatly reduces the tracking errors.**

I. INTRODUCTION

Laser Metal Deposition (LMD) is an additive manufacturing process wherein a laser is used to melt metal powder onto a substrate. In the LMD process, parts are fabricated in a layer by layer manner [1–2]. This allows direct fabrication of functional metal parts directly from CAD solid models, which reduces the machining and transportation cost, simplifies the product design, and facilitates mass customization. The LMD process can also be used to repair parts, thus reducing scrap and extending product service life.

A high quality deposition part should meet the following standards: high geometric precision, minimal porosity, and low dilution. The last two properties are directly related to melt pool temperature. Currently, the LMD process employs fixed process parameters (e.g., constant laser power, powder flow rate, travel speed). With fixed process parameters, the substrate temperature will increase as the process progresses, resulting in non–uniform track morphology, an increased Heat Affect Zone (HAZ), excessive dilution, thermal distortion, and cracking due to the build up of residual stress. Therefore, the development of an online temperature control system is of great value to improve part quality in LMD processes. Melt pool temperature control is also critical to the deposition of Functional Gradient Material parts, which requires accurate temperature control to form an even and tight bond between different materials. Without melt pool temperature control, cracks usually occur due to poor bonding.

There is very little research reported in the literature regarding temperature control in LMD processes. One method utilizes a PID controller designed based on a third order temperature model to control the melt pool temperature [3]. A constant temperature reference was used in the study. The melt pool temperature was measured with a two–color pyrometer capable of measuring temperatures in the range of 800–2500 °C. The results showed that temperature control can but not necessarily produce better quality clad layers compared to un–controlled cladding.

Melt pool temperature control requires a deposition process model describing the relationship between melt pool temperature and the process parameters (e.g., powder flow rate, laser power, traverse speed). Although there are several process models available in the literature [4–6], they are not suitable for online temperature control because of insufficient information for model computation or excessive model complexity. Therefore, an empirical model structure is employed in this paper. Based on the model, a melt pool temperature controller is designed. The performance is then verified experimentally.

This paper is organized as follows. Section 2 introduces the LMD system hardware. Section 3 formulates the melt pool temperature model and Section 4 presents the melt pool temperature controller design. In Section 5, experimental results are presented and discussed. Finally, in Section 6, the paper is summarized and concluding remarks are presented.

II. SYSTEM HARDWARE

The LMD system consists of the following components: 5–axis CNC machine, powder delivery system, diode laser, National Instruments (NI) real–time control system, laser displacement sensor, and temperature sensor. The system setup is shown in Figure 1. The diode laser (Nuvonyx ISL-1000M) has a maximum power output of 1000 W and a response time of 0.7 ms. The laser displacement sensor (OMRON, model Z4M–W100) has a measurement range of ±40 mm and a resolution of 8 μm. The temperature sensor (Mikron Infrared, model MI–GA 5–LO) has a measurement range of 400–2500 °C and a response time of 2 ms. The temperature sensor has a

978-1-4244-4524-0/09/$25.00 ©2009 AACC

resolution of 2.56 ℃. The temperature sensor is mounted on the nozzle and is used to measure the melt pool temperature during deposition. The control system is coded in NI LabVIEW and implemented on the real–time NI PXI system. A PXI 6040E multifunction board with a range of ±10 V and 12 bits of resolution is used for temperature measurement. A PXI 6711 analog output board with a range of ±10 V and 12 bits of resolution is used to input control signals to the laser amplifier.

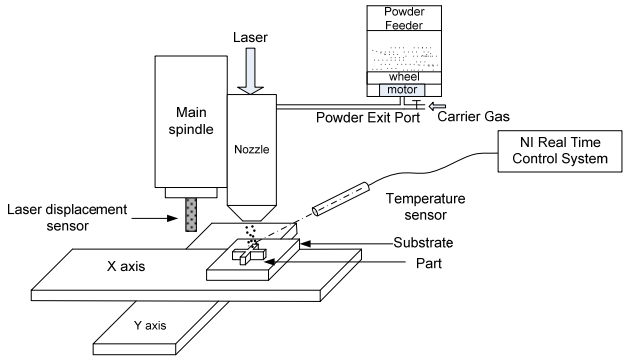

Figure 1: Laser metal deposition process system.

A. Melt Pool Temperature Modeling

Laser Metal Deposition is a complex process, which is governed by a large number of parameters. Among these parameters, powder flow rate, laser power, and traverse speed are typically employed to control the process properties. Therefore, the melt pool temperature is modeled using these three inputs.

The proposed melt pool temperature transfer function is

$$T(s)=\frac{K}{\tau s+1}V^{\alpha}(s)Q^{\beta}(s)M^{\gamma}(s) \tag{1}$$

where T is the melt pool temperature (℃), V is the traverse speed (ipm), Q is the laser power (W), M is the powder flow rate (g/min), K is the system gain, and τ is the time constant (s). The proposed model incorporates first order dynamics an the effects of major process parameters. The identification of the model parameters is separated into two steps:

a. Determine the model parameters (i.e., K, α, β, and γ) for the static process model, which is
$$T = Kv^{\alpha}q^{\beta}m^{\gamma} \tag{2}$$
b. Determine the time constant τ.

For step (1), a series of experiments, covering the process operation range, are designed using Design of Experiments (DOE). The model parameters in equation (2) are then estimated using method of Least Squares. The results are plotted in Figure 2(a). For step (2), an experiment where the laser power is incremented and decremented in a series of constant values is conducted. Recursive Least Squares is applied to estimate the time constant τ. The result is plotted in Figure 2(b). The estimated model parameters are listed in Table 1.

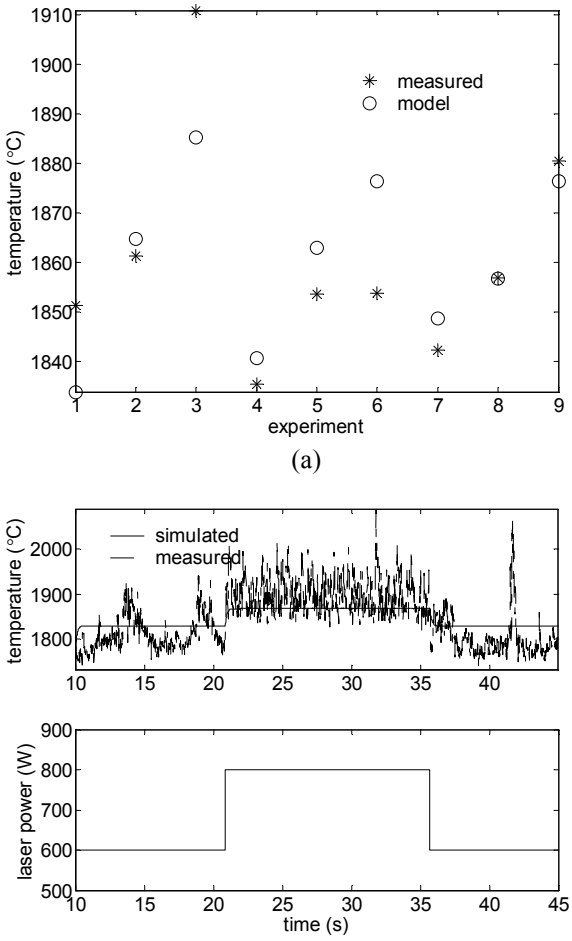

Figure 2: (a) Comparison between simulated temperature using static model and measured temperature and (b) Comparison between simulated temperature using dynamic model and measured temperature.

Table 1: Estimated model parameters.

Parameter	Value
K	1170
τ	0.115
α	$-8.18\cdot10^{-3}$
β	$7.16\cdot10^{-2}$
γ	$3.42\cdot10^{-3}$

The average error is

$$\bar{e}=\frac{100}{n}\sum_{i=1}^{n}\left|\frac{T_{model}(i)-T_{measured}(i)}{T_{measured}(i)}\right| \tag{3}$$

For the results in Figure 2, the average error is 2.06%. To validate the model, another laser power step test is conducted. The powder flow rate is 8 g/min and traverse speed is 6 ipm. The results are plotted in Figure 3. For this experiment, the average error is 2.59%. It can be observed that the simulated data matches the measured data quite well except some unmodeled dynamics.

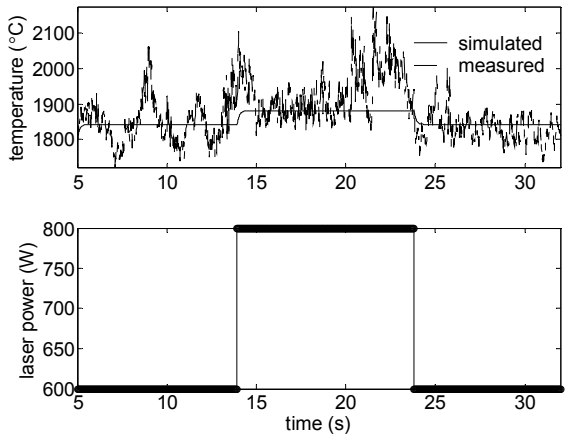

Figure 3: Comparison between the measured and simulated temperature.

III. CONTROLLER DESIGN

Letting $U(s)=V^{\alpha}(s)Q^{\beta}(s)M^{r}(s)$, equation (1) becomes

$$T(s)=\frac{K}{\tau s+1}U(s) \tag{4}$$

Transforming equation (4) into the discrete domain using a Zero Order Hold

$$\frac{T(z)}{U(z)}=\frac{b(z)}{a(z)}=\frac{K\left(1-e^{-T_s/\tau}\right)}{z-e^{-T_s/\tau}} \tag{5}$$

where T_s is the sample period (s). A general tracking controller using the Internal Model Principle is designed to control the temperature. The block diagram is shown in Figure 4. The laser and temperature sensor dynamics are neglected since the process time constant is much bigger than the laser and temperature sensor response time.

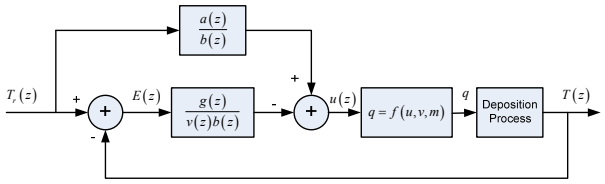

Figure 4: Melt pool temperature closed–loop control system block diagram.

The melt pool temperature reference is $T_r(z)$ and the error is $E(z) = T_r(z) – T(z)$. The control signal $U(z)$ is

$$v(z)b(z)U(z)=v(z)a(z)T_r(z)-g(z)E(z) \tag{6}$$

where $v(z) = z–1$ is the disturbance generating polynomial. This allows for integral action to account for the high degree of uncertainty in the model parameters and unmodeled dynamics. Since $a(z)T(z) = b(z)U(z)$, equation (6) becomes

$$\left[v(z)a(z)-g(z)\right]E(z)=0 \tag{7}$$

Thus the error dynamics can be shaped by selecting the controller polynomial $g(z)$. The closed–loop characteristic polynomial is $v(z)a(z)–g(z)$. In order to reduce the temperature oscillation, the characteristic polynomial is designed to have two poles located at $-e^{-T_s/\tau_1}$ and $-e^{-T_s/\tau_2}$, thus, the controller polynomial is

$$\begin{aligned} g(z)=g_1(z)+g_0= \\ \left(e^{-T_s/\tau_1}+e^{-T_s/\tau_2}-1-e^{-T_s/\tau}\right)z \\ +(e^{-T_s/\tau}-e^{-T_s/\tau_1-T_s/\tau_2}) \end{aligned} \tag{8}$$

Transforming equation (6) into a difference equation, the control signal is

$$\begin{aligned} u(k)=u(k-1)+K\left(1-e^{-T_s/\tau}\right)\left[T_r(k+1)-\right. \\ \left(1+e^{-T_s/\tau}\right)T_r(k)+e^{-T_s/\tau}T_r(k-1)- \\ \left.g_1e(k)-g_0e(k-1)\right] \end{aligned} \tag{9}$$

The laser power is

$$q(k)=\left(\frac{u(k)}{v(k)^{\alpha}\,m(k)^{r}}\right)^{1/\beta} \tag{10}$$

IV. EXPERIMENTAL STUDIES

To evaluate the performance of the melt pool temperature controller, two experiments are conducted. In the first experiment a constant temperature reference is utilized and in the other experiment the temperature reference varies with time. A Kalman filter is designed based on a stochastic process model to filter the temperature sensor feedback. The powder material used in the experiments is H13 tool steel with average particle diameter of 100 μm. The powder flow rate is set at 6 g/min and the traverse speed is 6 ipm.

A. Kalman Filter Design

It is observed that the temperature measurement signal has tremendous variations which may deteriorate the controller performance. Therefore a Kalman filter based on a first order stochastic model is designed to filter the measurement signal. The model is

$$\begin{aligned} \dot{x}(t)=\lambda x(t)+w(t) \\ y(t)=x(t)+\gamma(t) \end{aligned} \tag{11}$$

where x is the system state, λ is the system pole, w is a white noise signal with zero mean and covariance Q_w, y is the measurement, and γ represents the measurement noise with covariance R_γ.

To apply the Kalman filter, equation (11) is transformed into discrete form using a Zero-order hold

$$\begin{aligned} x(k+1)=A_z x(k)+w(k) \\ y(k)=x(k)+\gamma(k) \end{aligned} \tag{12}$$

where $A_z=e^{\lambda T_s}$.

The Kalman filter algorithm is implemented below. First the state and covariance respectively, are predicted by

$$\begin{aligned} \hat{x}^{p}(k+1)=A_z\hat{x}(k) \\ P^{p}(k+1)=A_zP(k)A_z^{T}+Q_w \end{aligned} \tag{13}$$

where $\hat{x}(k)$ and $P(k)$ are the estimated state and covariance at increment k, respectively. Second, the Kalman gain is updated by

$$K_g(k+1) = P^p(k+1)\left(P^p(k+1) + R_\gamma\right)^{-1} \quad (14)$$

where $K_g(k+1)$ is the Kalman gain at increment $k+1$. The last step is to update the state estimate and covariance with measurement $y(k+1)$

$$\begin{aligned} \hat{x}(k+1) &= \hat{x}^p(k+1) + K_g(k+1)\left(y(k+1) - \hat{x}^p(k+1)\right) \\ P(k+1) &= \left(1 - K_g(k+1)\right)P^p(k+1) \end{aligned} \quad (15)$$

The process and measurement covariances Q_w and R_γ need to be tuned experimentally. In this case, Q_w =25 and R_γ =2500.

To illustrate the effect the Kalman filter has on the measured temperature signal, an open–loop test is conducted with the laser power step test (the powder flow rate is set at 4 (g/min) and the traverse speed is 4 (ipm).). The filtered temperature signal is compared with the measured signal in Figure 5. To clearly show the comparison, a zoom–in version of the top subplot is provided in the bottom subplot.

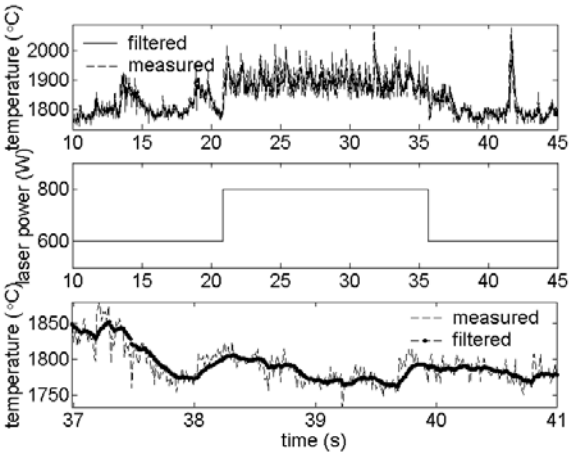

Figure 5: Plots of Kalman filter ($\lambda = -0.01$, R = 2500, Q = 25) open–loop test

It can be observed that with the Kalman filter, the magnitude of the variation becomes smaller. The variance of the measured temperature signal is 1540 (°C^2), while the variance of the filtered signal is 914 (°C^2). Therefore the variance is reduced by 40.7%.

B. Constant Temperature Reference

In this section, the melt pool temperature controller is used to track a constant temperature reference set at 1800 °C. Most LMD processes use fixed process parameters, and acceptable process parameters are found through a lengthy trial and error process. In this section, the experimental results using the temperature controller will be compared to open–loop results where the laser power trajectory is designed based upon the model. According to the model developed above, the laser power should be 439 W for a melt pool temperature of 1800 °C. The open–loop experimental results are shown in Figure 6. The average melt pool temperature is 1770 °C, the average absolute error is 65 °C, and the error standard deviation is 60 °C.

In the next experiment the temperature controller designed above is implemented. The results are shown in Figure 7. The average melt pool temperature is 1800 °C, the average absolute error is 20 °C, and the error standard deviation is 25 °C. Compared with the results using constant process parameters, the average absolute error is reduced by 70.0% and the error standard deviation is reduced by 59.5%. The results show that the temperature controller works well when tracking a constant temperature reference and significantly reduces the temperature error and variation when compared to experiments with constant process parameters.

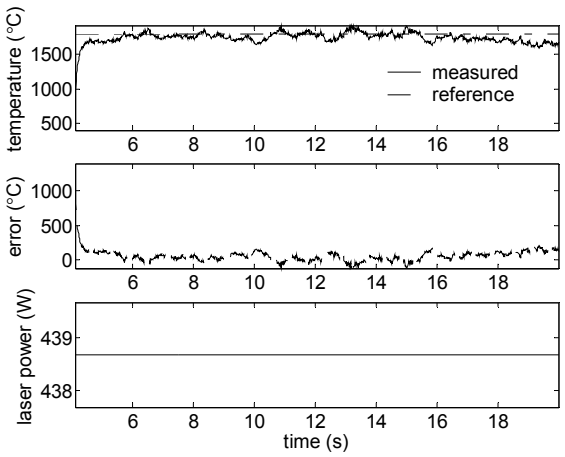

Figure 6: Open–loop temperature response for $T_r(t)$ = 1800 °C.

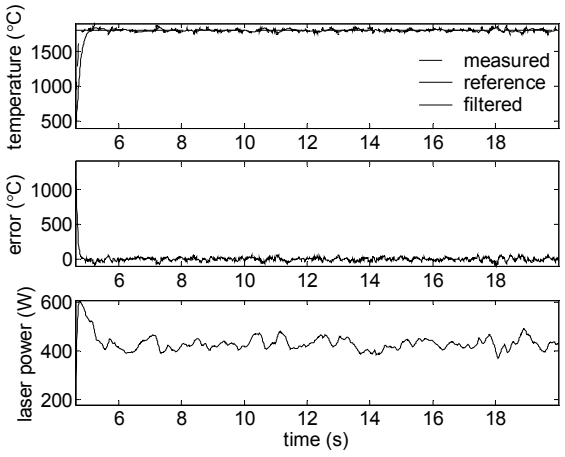

Figure 7: Closed–loop temperature response for $T_r(t)$ = 1800 °C.

C. Time Varying Temperature Reference

In this section, the melt pool temperature controller is used to track a time varying temperature reference. The temperature reference signal for this experiment is

$$T_r(t) = 1850 + 50\sin(t) \tag{16}$$

The experimental results using the temperature controller are compared to open–loop results where the laser power trajectory is designed based upon the model. The open–loop experimental results are shown in Figure 8. The average absolute error is 135 °C and the error standard deviation is 130 °C.

In the next experiment the temperature controller designed above is implemented. The results are shown in Figure 9. The average absolute error is 25 °C and the error standard deviation is 30 °C. Compared with the results when tracking a constant temperature reference, the average error and error standard deviation are slightly larger. Compared with the controller using a predefined laser power trajectory, the average absolute error decreased by 82.5% and the error standard deviation decreased by 76.8%. The results show that the temperature controller works well when tracking a time varying temperature reference and significantly reduces the temperature error and variation when compared to experiments with predefined process parameters based on the empirical model.

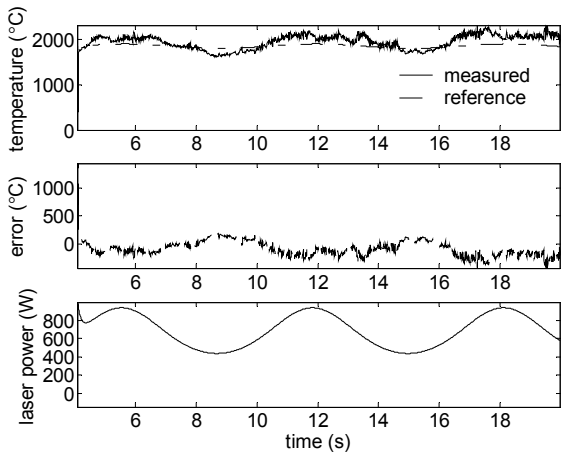

Figure 8: Open–loop temperature response for $T_r(t)$ = 1850 + 50sin(t) °C.

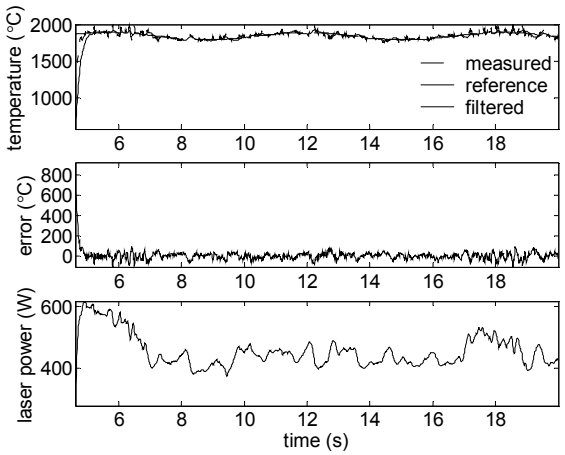

Figure 9: Closed–loop temperature response for $T_r(t)$ = 1850 + 50sin(t) °C.

V. SUMMARY AND CONCLUSIONS

To control the melt pool temperature in LMD processes, an empirical process model describing the relationship between the temperature and laser power, powder flow rate, and traverse speed was established and verified experimentally. A general tracking controller using the Internal Model Principle was then designed to control the temperature. To test the controller performance, two experiments, which are designed to track a constant temperature reference and a time varying temperature reference, were conducted. The results show the melt pool temperature controller performs well in tracking both of these references. The affect of melt pool temperature control on deposition microstructure will be investigated in future studies.

ACKNOWLEDGEMENT

The authors would like to acknowledge the financial support of the Intelligent Systems Center at Missouri University of Science and Technology.

REFERENCES

[1] Choi, J., 2002, "Process and Prosperities Control in Laser Aided Direct Metal/Materials Deposition Process," *Proceedings of IMECE*, New Orleans, Louisiana, November 17–22, pp. 1–9.

[2] Griffith, M.L., Keicher, D.M., Atwood, C.L., Romero, J.A., Smegeresky, J.E., Harwell, L.D., and Greene, D.L., 1996, "Free Form Fabrication of Metallic Components Using Laser Engineered Net Shaping (LENS)," *Solid Freeform Fabrication Symposium*, August 12–14, Austin, Texas, pp. 125–131.

[3] Salehi, D. and Brandt, M., 2006, "Melt Pool Temperature Control using LabVIEW in Nd:YAG Laser Blown Powder Cladding Process," *International Journal of Advanced Manufacturing Technology*, Vol. 29, pp. 273–278.

[4] Doumanidis, C. and Kwak, Y–M., 2001, "Geometry Modeling and Control by Infrared and Laser Sensing in

Thermal Manufacturing with Material Deposition," *ASME Journal of Manufacturing Science and Engineering*, Vol. 123, pp. 45–52.
[5] Han, L., Liou, F.W., and Musti, S., 2005, "Thermal Behavior and Geometry Model of Melt Pool in Laser Material Process," *Journal of Heat Transfer*, Vol. 127, pp. 1005–1014.
[6] Pinkerton, A.J. and Li, L., 2004, "Modelling the Geometry of a Moving Laser Melt Pool and Deposition Track via Energy and Mass Balances," *Journal of Physics D: Applied Physics*, Vol. 37, pp. 1885–1895.